

Synthesis, Crystal structure, Optical, Dielectric properties and Theoretical calculations of L-Phenylalanine Maleic Acid for Nonlinear Optical Applications

K. Deepa¹, S. Senthil² and J. Madhavan^{1*}

¹Department of Physics, Loyola College, Chennai, Tamil Nadu, India

²Department of Physics, Government Arts College for Men, Nandanam, Chennai, Tamil Nadu, India

ABSTRACT

Single crystals of L-phenylalanine maleic acid [LPM] with reasonable size have been grown by slow evaporation solution growth method. Quantum chemical calculation of L-phenylalanine maleic acid [LPM] was carried out by using DFT/B3LYP/6-31pG(d,p) method. The powder X-ray diffraction pattern was recorded and indexed. Both the experimental and theoretical vibrational spectrum validates the presence of functional groups. Polarizability, first order hyperpolarizability and the electric dipole moment values have been computed theoretically. TG/DTA analysis has been employed to understand the thermal and physio-chemical stability of the title compound. Frequency conversion property of the crystal was tested by Kurtz and Perry method. Dielectric constant and dielectric loss of picolinium maleate are measured in the frequency range from 50 Hz to 5 MHz at room temperature. Optical absorption behavior of the grown crystal was examined by recording the optical spectrum and band gap energy was also estimated. The calculated HOMO and LUMO energy shows the charge transfer nature of the molecule.

Keywords. Powder XRD, optical absorption, Density Functional Theory, HOMO-LUMO analysis, FTIR, SHG efficiency.

I. INTRODUCTION

Photonics is playing an ever-increasing role in today's technology by efficiently replacing electronics in electro optic devices. Mulliken's theory of charge transfer interactions between an electron donor and electron acceptor has been successfully applied to many interesting studies. These complexes have attracted great attention for nonlinear optical materials and electrical conductivities [1-5]. The bond between the donor and acceptor is formed by the interaction between the electron poor ring of the picric acid and electron rich ring of benzophenone. Picric acid also forms charge transfer complexes with pyridine, piperidine and amines [6-9]. The organic materials with benzophenone, which are of great applications for second and third order nonlinear

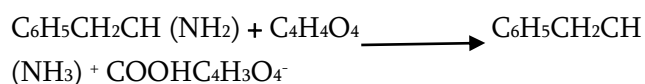
optical properties due to their high nonlinearity with good electronic response. According to the concepts of the molecular and crystal technology, the organic molecules offer many possibilities to tailoring the substances with desired properties through optimization of the microscopic hyperpolarizabilities and the incorporation of the molecules in a crystalline lattice [10-12].

NLO properties of the crystals get affected due to the influence of hydrogen bonding on dipole alignment [13]. Among the available materials, nitro compounds receive much attraction because of its high NLO coefficients [14, 15]. 2-Methyl, 5-dinitrobenzoic acid (MDNBA) is an aromatic compound has both electron donor group (carboxyl) and electro acceptor groups (methyl

&nitro) hence there may be a possibility for the formation of hydrogen bonds in this system. This push pull system with weak hydrogen bonds may show high value of NLO coefficients. In the present work, we report the experimental and theoretical investigation of L-Phenylalanine maleate (LPM) single crystal. Phenylalanine, an essential amino acid commonly found in proteins, plays a key role in the formation of variety of physiologically important chemicals that transmit signals between nerve cells besides possessing excellent NLO properties.

II. EXPERIMENTAL PROCEDURE

High purity L-phenylalanine (Merck 99%) and maleic acid (AR grade) were taken in 1.1 molar ratio and dissolved in deionized water. The reaction is as follows,



the synthesized salt is purified by successive recrystallization process. The solubility for LPM was determined by dissolving the recrystallized salt in deionized water in an air tight container maintained at a constant temperature with continuous stirring. After attaining the saturation, the equilibrium concentration of the solute was analyzed gravimetrically. The same procedure is repeated for different temperatures from 30 to 55 °C at intervals of 5 °C. Figure 1 gives the solubility curve of LPM. The saturated solution is prepared for the growth of LPM single crystals according to solubility data. After a period of 25 days, optically good quality single crystals of dimension upto 18 x 5 x 4 mm³ are harvested. The photograph of as grown single crystals of LPM crystal is shown in Figure 2.

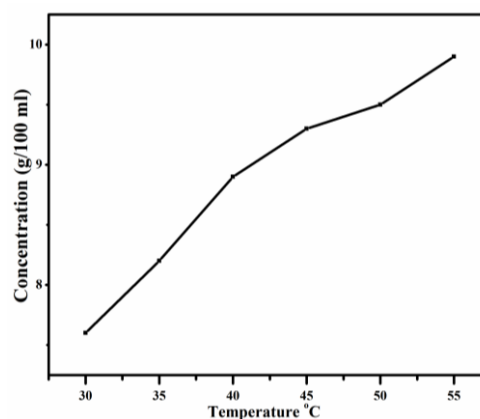


Figure 1. Solubility curve of LPM

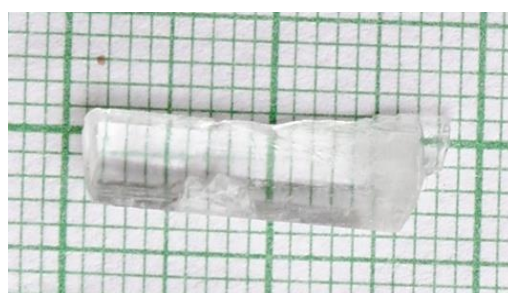


Figure 2. Photograph of as grown LPM single crystal

III. RESULTS AND DISCUSSION

3.1 Single crystal XRD Analysis

The grown crystal was subjected to single crystal X-ray diffraction study at room temperature. From the single crystal analysis it was observed that the crystal belongs to monoclinic crystal system having non-centro symmetry with P2₁ space group. The crystal data and structural refinement data are given in Table 1. In the crystal structure of LPM single crystal amino acid molecule exists in the cationic form with a positively charged amino group and an uncharged carboxylic acid group. In the title compound, C₉H₁₂NO₂⁺C₄H₃O₄⁻, the amino acid molecule exists in the cationic form and the maleic acid molecule in the mono-ionized state. In the semi-maleate anion, a nearly symmetric intra molecular O-H...O hydrogen bond is observed. The phenylalaninium cations and the semimaleate anions form hydrogen-bonded double chains and are held

together by N-H...O hydrogen bonds. Theoretically Simulated XRD pattern of LPM single crystal with indexed peak is given in Figure 3. Experimental Powder XRD pattern is also shown in Figure 4. Both XRD patterns are almost similar in comparison.

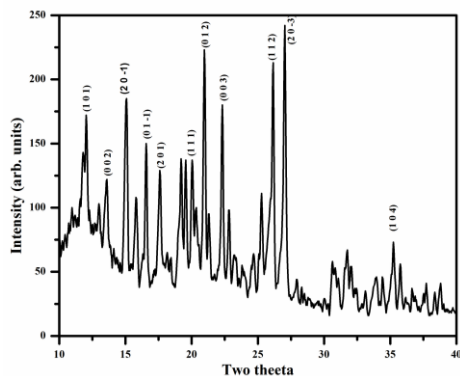


Figure 3. Experimentally obtained Powder XRD pattern of LPM

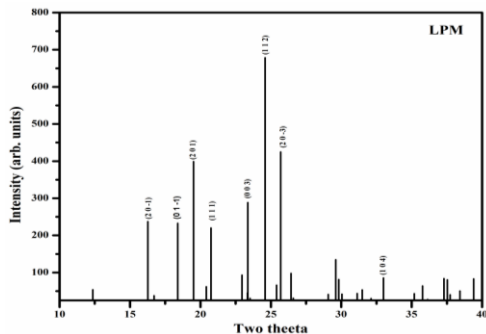


Figure 4. Theoretically simulated powder XRD pattern of LPM.

Table 1. Crystal parameters of LPM

Empirical Formula	C ₁₃ H ₁₅ NO ₆
Formula weight	281.26
Temperature	293(2)
Wave length	1.54180
Crystal system, Space group	monoclinic, P2 ₁
Unit cell dimensions	a=11.0560(3)Å β=101.070 b=5.3326(4) Å γ = c=11.4712(6) Å 90.000°
Cell volume	663.73(4)Å ³
Calculated Density	1.413 g/cm ³
Absorption coefficient	0.957 mm ⁻¹

F(000)	296
Crystal size	.25 x.23 x.19mm ³
Theta range for data collection	3.93 to 67.92deg.
Limiting indices	-13<=h<=0, 0<=k<=6, -13<=l<=13
Reflections collected/unique	1353/1294 [R(int)=0.0000]
Completeness to theta = 67.92	100%
Refinement method	Full-matrix least squares on F ²
Data/restraints/parameters	1353/1/187
Goodness- of – fit on F ²	1.13
Final R indices [I>2sigma(I)] 80	R1=0.028, wR2 =0.0693
R indicies (all data)	R1=0.030, wR2 =0.078
Extinction coefficient	0.052(3)

3.2 Computational details

Quantum chemical Density functional theoretical (DFT) computations were performed using closed-shell Becke–Lee–Yang–Parr hybrid exchange–correlation three–parameter functional (B3LYP) in combination with 6-31G (d,p) basis set to derive the complete geometry optimizations and normal-mode analysis on isolated entities. Above said task was achieved using Gaussian03W [16]. The optimized geometries corresponding to the minimum potential energy surface have been obtained by solving self consistent field (SCF) equation iteratively. The absence of imaginary values of wave numbers on the calculated vibrational spectrum confirms that the structure deduced corresponds to minimum energy.

3.2.1 Molecular geometry

The optimized molecular structure of the isolated LPM molecule calculated using DFT theory at B3LYP/6-31 level is shown in Figure 5.

The optimized C–C bond lengths in LPM fall in the range 1.39471–1.54000 Å. These values show that our calculation results are more consistent with the experimental data. The calculated bond length of C₁–C₂ and C₁–C₆ are 1.39516 and 1.39483 Å. This shows negligible conjugation between the aromatic ring system and the rest of the molecule. The ring twisting influences the delocalization of the π* electrons and can explain the changes of optical properties of L-Phenylalanine relative to the electronic properties of the substituent. The geometrical parameters, H₂₄⋯O₂₂ (1.25000 Å) and O₂₃⋯H₂₄ (1.38000 Å) are well within hydrogen bonding limit and shows O–H⋯O hydrogen bonding. These distances are shorter than the sum of the Van der Waal’s radii (1.2 Å for H and 1.52 Å for O) because the hydrogen bridge tends to push the two hetero atoms closer to each other. Although theoretical results are not exactly close to the experimental values for the compounds, they are generally accepted that bond lengths and bond angles depend on the method and the basis set used in the calculations, and they can be used as foundation to calculate the molecular properties for the compounds.

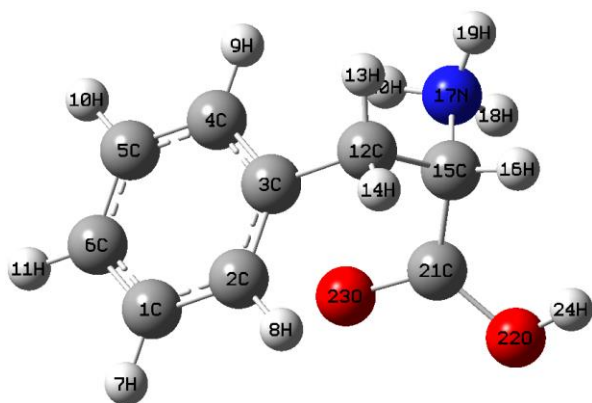


Figure 5. Atomic numbering system adapted for ab initio.

3.2.2 Hyperpolarizability studies

The ab initio calculated non-zero μ value shows that this compound might have microscopic first static hyperpolarizabilities with non-zero values obtained by the numerical second-derivative of the electric dipole moment according to the applied field strength. The magnitude of molecular hyperpolarizability,

presence of the number of chromophores and the degree of noncentrosymmetry are the deciding criteria of the second order susceptibility χ⁽²⁾ values in an NLO system. A large value of the first hyperpolarizability is the prerequisite to behave as a good NLO material, and the important parameters influencing β generally are (i) donor–acceptor system, (ii) nature of substituents, (iii) conjugated π system and (iv) the influence of planarity. The first-order hyperpolarizability (β) of this novel molecular system of LPM were calculated using B3LYP with 6-31G (d,p) basis sets, based on the finite field approach. In the presence of an applied electric field, the energy of a system is a function of the electric field. The first hyperpolarizability is a third-rank tensor that can be described by a 3 × 3 × 3 matrix. The 27 components of the 30 matrix can be reduced to 10 components due to the Kleinman symmetry. Relation connecting non linear response, linear polarizability(α_{ij}) and first order hyperpolarizability(β_{ijk}) can be represented as a Taylor expansion of the total dipole moment as

$$\mu_t = \mu_0 + \alpha_{ij} E_i + \beta_{ijk} E_i E_j + \dots \quad (1)$$

The components of first order hyperpolarizability can be determined using the relation

$$\beta_{ij} = \beta_{iii} + \frac{1}{3} \sum_{i \neq j} (\beta_{ijj} + \beta_{jij} + \beta_{jji}) \quad (2)$$

Using the x,y and z components the magnitude of first order hyperpolarizability (β_{tot}) tensor can be calculated by the following equation

$$\beta_{tot} = (\beta_x^2 + \beta_y^2 + \beta_z^2)^{1/2} \quad (3)$$

The complete equation for calculating the first order hyperpolarizability from GAUSSIAN 03 output is given as

$$\beta_{tot} = (\beta_{xxx} + \beta_{xyy} + \beta_{xzz})^2 + (\beta_{yyy} + \beta_{yzz} + \beta_{yxx})^2 + (\beta_{zzz} + \beta_{zxx} + \beta_{zyy})^2 \quad (4)$$

The β components of GAUSSIAN 03 output are reported in atomic units and the calculated values have to be converted into electrostatic units (1 a.u = 8.3693 × 10⁻³³ esu). The calculated first order hyperpolarizability values for LPM molecule are given in Table 2.

Table 2. Hyperpolarizability of LPM in esu

β_{xxx}	32.86638
β_{xxy}	-10.47789
β_{xyy}	2.415801
β_{yyy}	-13.458078
β_{xxz}	-0.522343
β_{xyz}	-14.636601
β_{yyz}	-80.96379
β_{zzz}	24.894204
β_{yzz}	-16.27824
β_{zzz}	-116.6978
β_{tot}	1.765808×10^{-30}

3.2.3 HOMO-LUMO Analysis

The energies of the highest occupied molecular orbital (HOMO) and the lowest unoccupied molecular orbital (LUMO) are computed at B3LYP/6-31G(d, p) level. HOMO and LUMO orbitals are shown in Figure 6. Generally, the energy values of LUMO, HOMO and their energy gap reflect the chemical activity of the molecule. HOMO as an electron donor represents the ability to donate an electron, while LUMO as an electron acceptor represents the ability to receive an electron. The smaller the LUMO and HOMO energy gaps, the easier it is for the HOMO electrons to be excited. The indication of charge transfer from L-phenylalaninium to maleate moiety through the hydrogen bond, which is an important requirement to obtain large second order NLO response. The energies of the HOMO and LUMO, based on the optimized structure are computed as -0.10814 and -0.05570 a.u., respectively. The HOMO-LUMO energy gap is -0.05244 a.u. The calculated HOMO and LUMO energies clearly show that charge transfer occurs within the molecule.

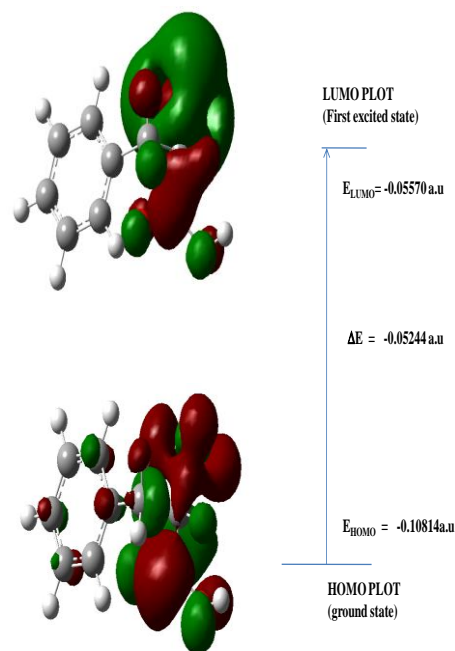


Figure 6. HOMO – LUMO plot of LPM molecule.

3.3 Vibrational Analysis

IR spectroscopic analysis is an important tool to characterize material structure. The IR spectrum of LPM crystal mainly arises from phenyl group, nitro group, carboxyl group, water molecule, etc. As a widespread inter- or intra-molecular force, hydrogen bond has tremendous effect on the shift of IR spectrum [17]. In general the influence of the strong hydrogen bonds on the nonlinear properties of the molecule can be considered, thus the vibrational spectra can be helpful in the elucidation of the role of hydrogen bond in the structure of the crystal exhibiting nonlinear optical properties. The experimental IR spectrum is compared with the results of B3LYP/6-31G (d, p) calculation carried out for the studied compound. Some bands in calculated IR spectra were not observed in the experimental spectrum.

It is important to note that computed wave numbers correspond to gaseous phase of isolated molecular state whereas the observed wave numbers correspond to the solid state spectra. FT-IR spectrum of the grown

crystal was recorded in the range 400 cm^{-1} to 4000 cm^{-1} , using KBr pellet technique on BRUKKER IFS FT-IR Spectrometer. Recorded FT-IR spectrum and theoretically simulated IR spectrum of the LPM molecule are shown in Figs.7 and 8. It is found that LPM molecule has 24 moiety and is in stable conformation with C_1 symmetry then exhibits 66 normal modes of vibrations. The normal modes of LPM is distributed amongst the symmetry species as $\Gamma_{3N-6} = 45A'$ (in-plane) + $21A''$ (out-of-plane) respectively. All the vibrations are active in Infrared vibrations. The detailed fundamental modes of vibrational assignments with the observed, calculated frequencies, IR intensities, reduced mass and force constants of LPM molecule is presented.

3.3.1 O–H Vibrations

The O–H group gives rise to three vibrations (stretching, in-plane bending and out-of-plane bending vibrations). The O–H group vibrations are likely to be the most sensitive to the environment, so they show pronounced shifts in the spectra of the hydrogen bonded species. The hydroxyl stretching vibrations are generally observed in the region around 3500 cm^{-1} .

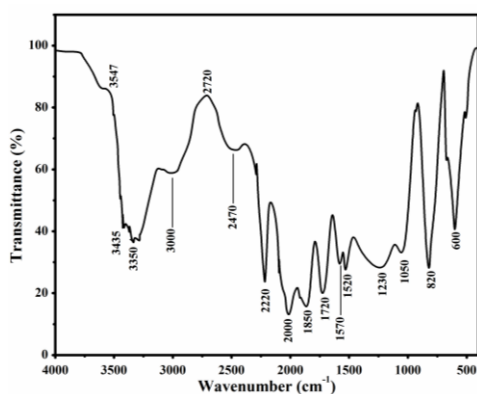


Figure 7. Experimentally obtained FTIR spectrum of LPM

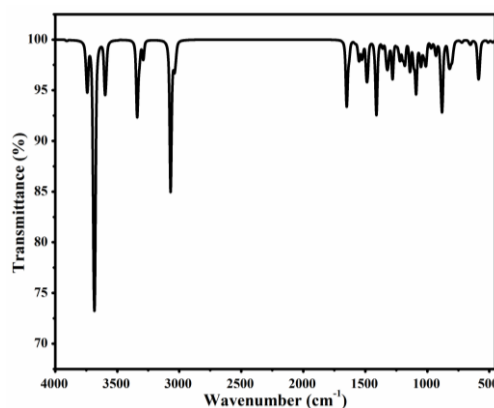


Figure 8. Theoretically simulated FTIR spectrum of LPM

In the case of the un-substituted phenols it has been shown that the frequency of O–H stretching vibration in the gas phase is 3657 cm^{-1} . Similarly in our case a very strong FT-IR bands at 3905 , 3743 and 3684 cm^{-1} are assigned to O–H stretching vibrations. The hydrogen bonding effect through hydroxyl group leads to dimer conformation OH stretching mode calculated at 3595 cm^{-1} which is much closer to the FT-IR experimental observation at 3547 cm^{-1} . The O–H in-plane bending vibration in the phenols, in general lies in the region $1150\text{--}1250\text{ cm}^{-1}$ and is not much affected due to hydrogen bonding unlike to stretching and out-of-plane bending frequencies. The weak band in FT-IR spectrum at 1102 cm^{-1} is assigned to O–H in plane bending vibration. The theoretically computed value at 1090 cm^{-1} by B3LYP method shows good agreement with recorded spectrum. The O–H out-of-plane bending mode for the free molecule lies below 300 cm^{-1} and it is beyond the infrared spectral range of the present investigation. However, for the associated molecule the O–H out-of-plane bending mode lies in the region $517\text{--}710\text{ cm}^{-1}$ in both intermolecular and intramolecular associations, the frequency is at a higher value than in free O–H [18]. In our present investigation a strong band observed in FT-IR spectrum at 650 cm^{-1} is assigned to O–H out-of-plane bending vibration, the theoretically computed value by B3LYP also shows the same kind of vibrations in the region $651, 405$ and 296 cm^{-1} are assigned to O–H out-of-plane bending vibration.

3.3.2 C-N Vibrations

The C-N ring stretching vibration bands occur in the region on 1600- 1500 cm⁻¹. The present molecule exhibits this vibration in IR spectrum at 1650cm⁻¹ and the theoretically computed value at 1650cm⁻¹ by B3LYP method shows good agreement with recorded spectrum. C-N stretching absorption assigned in the region 1382–1266 cm⁻¹. In the present work, the band observed at 1113 cm⁻¹ in FT-IR spectrum has been assigned to C–N stretching vibration. The calculated frequency at 1012 cm⁻¹ is in good agreement with experimental value. Frequency band observed at 723cm⁻¹ by theoretical calculation is assigned to CN out plane bending and band at 600 cm⁻¹ in experimental spectrum is due to CN in plane deformation. Calculated band at 177 cm⁻¹ is assigned to CN in plane bending.

3.3.3 C-O Vibrations

The C-O stretching vibration for this LPM molecule is obtained at 1380 and 1230cm⁻¹ in IR spectrum. Both the bands well coincided with theoretically calculated values at 1326 and 1223 cm⁻¹ using B3LYP method. The band occurred at 216 cm⁻¹ is assigned to C-O out plane bending occurred. The lowering of C-O stretching mode is attributed to the fact that the C-O group chelate with the other nucleophilic groups, thereby forming both intra and intermolecular hydrogen bonding in the crystal.

3.4 Optical Properties of LPM

The optical properties of a material are important, as they provide information on the electronic band structures, localized states and types of optical transitions. To determine the transmission range and hence to know the suitability of LPM single crystals for optical applications, the UV–Vis-NIR spectra (Figure 9) were recorded in the range of 200–1200 nm. The UV-Vis-NIR spectrum gives information about the structure of molecule because the absorption of UV and visible light involves the promotion of the

electrons in the σ and π orbitals from the ground state to higher energy states.

The spectrum reveals that the LPM compound has a wide transparency window in the region 240–1000 nm (~80%) and shows no remarkable absorption in the visible region. This data was further used for analyzing optical band gap energy (E_g) using the formula for optical absorption of

$$(\alpha h\nu) = k (h\nu - E_g)^{n/2} \quad (3.1)$$

n is an integer equal to 1 for a direct band gap and 4 for an indirect band gap. The values of the direct optical band gap E_g were obtained from the intercept of $(\alpha h\nu)^2$ versus $h\nu$ curve plotted in Figure 10. Ideally the graph should be linear the deviation from linearity at low incident photon energy can be attributed to the presence of irregularities and imperfection of the crystals. The intercept obtained by the extrapolation of the linear portion of the plot to energy axis gives the band gap energy of the crystal. The band gap is found to be 4.5 eV. The other optical constants were calculated using the following theoretical formulae. The optical properties of the crystals are governed by the interaction between the crystal and the electric and magnetic fields of the electromagnetic waves. Extinction coefficient is the fraction of light lost due to scattering and absorption per unit distance in a participating medium. In electromagnetic terms, the extinction coefficient can be explained as the decay or damping of the amplitude of the incident electric and magnetic fields.

The extinction coefficient in terms of absorption coefficient is obtained as

$$K = \frac{\alpha \lambda}{4\pi} \quad (3.2)$$

The Reflectance is derived as a function of absorption coefficient as

$$R = \frac{1 \pm \sqrt{(1 - \exp(-\alpha d) + \exp(\alpha d))}}{1 + \exp(-\alpha d)} \quad (3.3)$$

And the linear refractive index is given by

$$n = \frac{-(R+1) \pm \sqrt{-3R^2 + 10R - 3}}{2(R-1)} \quad (3.4)$$

Then the complex dielectric constant is related to refractive index and the extinction coefficient as

$$\epsilon_c = \epsilon_r + \epsilon_i \quad (3.5)$$

Where the real and imaginary part of dielectric constant is

$$\epsilon_r = n^2 - K^2 \quad (3.6)$$

$$\epsilon_i = 2nK \quad (3.7)$$

The optical conductivity as a function of frequency response of the material when irradiated with light is calculated as

$$\sigma_{op} = \frac{\omega n c}{4\pi} \quad (3.8)$$

where c is the velocity of light. The electrical conductivity can also be estimated by optical method using the relation

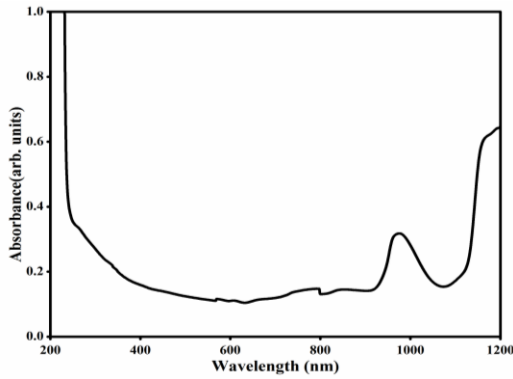


Figure 9. Optical absorption spectrum of LPM

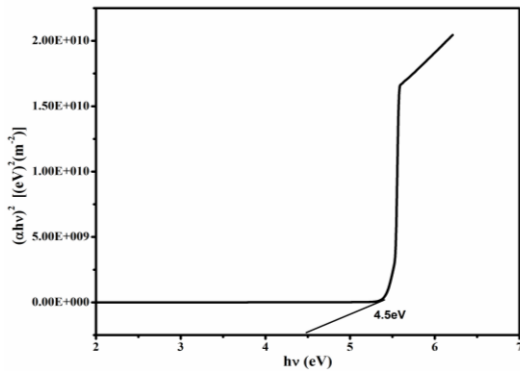


Figure 10. Energy band gap of LPM

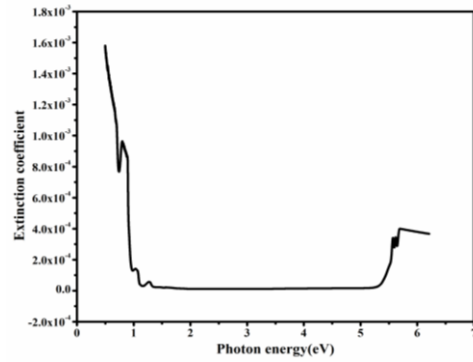


Figure 11. Extinction coefficient Vs Incident Photon Energy of LPM

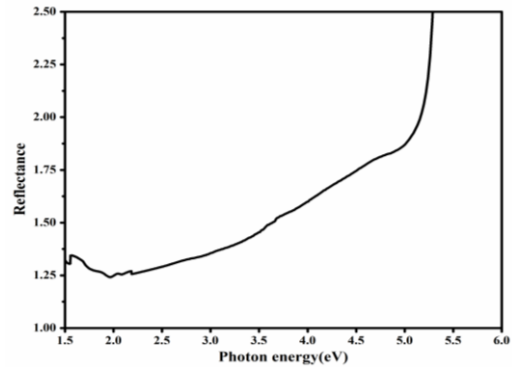


Figure 12. Reflectance Vs Incident photon energy of LPM

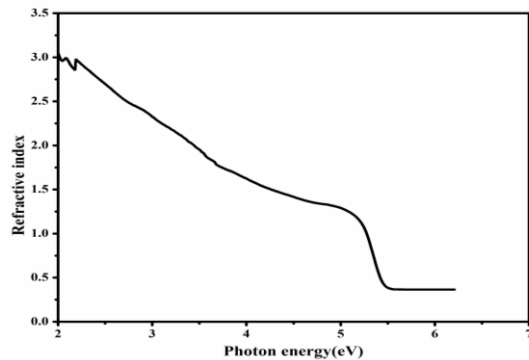


Figure 13. Refractive index Vs Incident photon energy of LPM

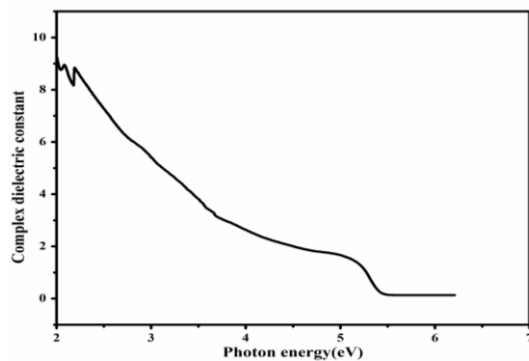


Figure 14. Complex dielectric constant Vs Incident photon energy of LPM

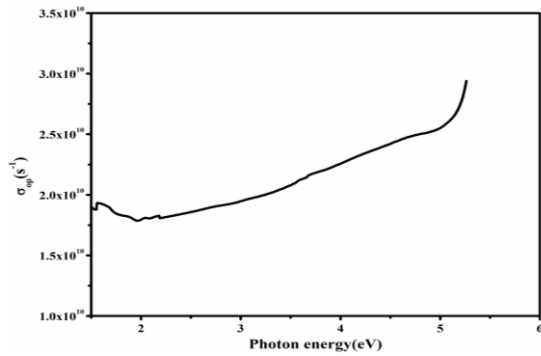


Figure 15. Optical conductivity Vs Incident photon energy of LPM.

$$\sigma_e = \frac{2\lambda\sigma_{op}}{\alpha} \quad (3.9)$$

Figure 11 & Figure 12 shows the plot of extinction coefficient and reflectance against incident photon energy. It's found that extinction coefficient remains constant for incident photon energy of 1.2 eV to 5.5 eV and reflectance increases linearly with photon energy. Figure 13 depicts the variation of refractive index with incident photon energy. Initially the refractive index decreases with increasing photon energy then becomes constant. Variation of complex dielectric constant and optical conductivity of the material with incident photon energy is analysed from Figure 14 and Figure 15. The high optical conductivity (10^{10}) confirms the high photo response nature of the material.

3.5 Thermal studies

The thermogravimetric analysis was carried out for the initial sample weight of 5mg, by subjecting to a temperature range of 50–800°C at a heating rate of 20°C/min in the nitrogen atmosphere. From the TGA curve (Figure 16), it is clear that the material is stable up to 130°C before decomposition starts. In TGA, decomposition takes place after 151°C as the first stage. It goes up to 240°C which may be due to the loss of C_2H_4 and $2CO_2$, resulting in a loss of weight of 18.36%. Another weight loss of 36.71% at the second stage, noticed between the temperatures. 250–350°C is due to the expulsion of C_6H_5 , CH_2 and NH_3 . The next stage of decomposition results in a loss of 27.54% between the temperature range 340–500°C is due to the release

of CO_2 . The next stage of decomposition results in a loss of 27.54% between the temperature range 500–800°C is due to the release of CO. The remaining residue corresponds to carbon of the LPM crystal. The sharp DTA peaks at 180 and 300 °C are attributed to the decomposition of the material, which match well with the first and second stage of decomposition in the TGA curve, respectively.

3.6 NLO studies

Preliminary study of the powder SHG conversion efficiency was carried out with Nd:YAG laser beam of wavelength 1064 nm, using Kurtz and Perry method. Nd:YAG laser beam of wavelength 1064nm was used with an input power of 2.33 mJ per pulse. The crystals of LPM were ground to a uniform particle size of about 125–150 nm and packed in capillaries of uniform bore and exposed to the laser radiation.

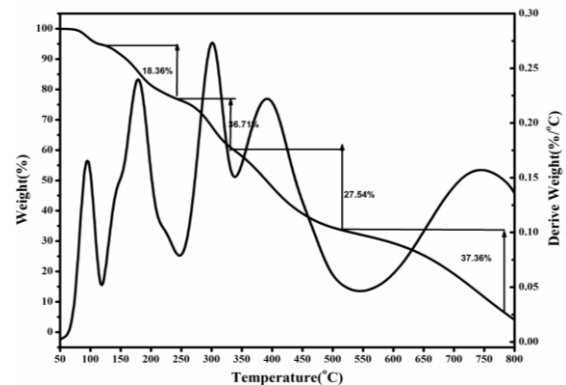


Figure 16. TG-DTA curves of LPM single crystals

A powder of KDP with same particle size was used as the reference material in the SHG measurement. The output from the sample was allowed through a monochromater to collect the intensity of 532nm components and eliminate fundamental. The generation of second harmonic was focused by a lens and detected by the photomultiplier tube. The generation of the second harmonic was confirmed by the emission of green light (532 nm). The SHG signal of 190 mV was obtained. The standard potassium dihydrogen phosphate (KDP) crystal gave a SHG signal of 130mV per pulse for the same input energy.

The conversion efficiency of the LPM crystal is found to be 1.5 times that of standard potassium dihydrogen phosphate (KDP) crystal.

3.7 Dielectric Studies

The Dielectric properties were carried out at room temperature for frequencies varying from 50Hz to 5MHz. The capacitance (c) and dissipation factor (d) of the parallel plate capacitor were measured. The dielectric constant and dielectric loss are calculated using the equations

$$\epsilon' = \frac{Cd}{\epsilon_0 A}$$

Where A is the area of the sample and d is the thickness of the sample and ϵ_0 is the permittivity of free space. The frequency dependence of the dielectric constant is shown in Figure 17. It is found that the dielectric constant of LPM is high at low frequencies and it decreases with increasing frequency. The high value of dielectric constant is attributed to high ionic conductivity. The dielectric constant decreases with increasing frequency and becomes almost saturated beyond 2 kHz. Figure 18 shows the exponential decrease of dielectric loss ($\tan \delta$) of LPM as a function of frequency along (001) orientation. The low value of dielectric loss indicates that the grown crystals are good in quality. The larger values of dielectric loss at lower frequency may be attributed to space charge polarization owing to charge lattice defect. The characteristic of low dielectric constant and dielectric loss with high frequency for a given sample suggests that the sample possesses enhanced optical quality with lesser defects and this parameter is of vital importance for various nonlinear optical materials and their applications.

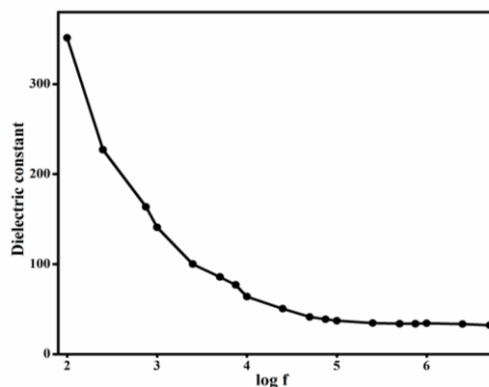


Figure 17. Variation of dielectric constant of LPM

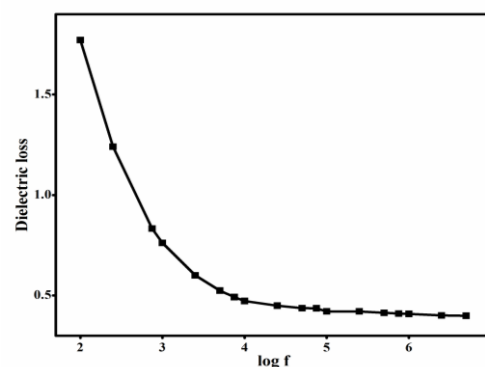


Figure 18. Variation of dielectric loss of LPM

IV. CONCLUSION

Optically good quality single crystals of LPM were grown by slow solvent evaporation technique. The crystalline nature of grown crystal is confirmed by single crystal X-ray diffraction analysis and it is found that the crystal belongs to the monoclinic system with $P2_1$ space group. Density functional theory (DFT) computations using (B3LYP) level with 6-31G (d,p) basis set gives optimized structure parameters of LPM molecule. It is understood that hydrogen bonds are prevalent in this material and the optimized C–C bond lengths of LPM fall in the range 1.39471–1.54000 Å. The magnitude of molecular first order hyperpolarizability for this molecule is in suitable range to exhibit NLO behavior. Molecular energy gap of LPM was found as -0.05244 au by HOMO-LUMO analysis. Theoretically calculated vibrational frequencies are compared with experimentally obtained FT-IR frequencies. Spectral assignments are carried out for various vibrational frequencies. Force

constants and reduced masses also calculated for all moieties of LPM molecule. Optical absorption spectrum was recorded for the given crystal and it is found that it has minimum absorption between 240 - 1000 nm. The optical band gap of the material is found as 4.5 eV. Various linear optical constants like extinction coefficient, reflectance, refractive index, complex dielectric constant and optical conductivity are calculated and related with incident photon energy. This optical analysis reveals the NLO behavior of the material. Mechanical strength, Thermal stability and SHG studies were carried out and the conversion efficiency of the LPM crystal is found to be 0.27 times that of KDP crystal. Low values of dielectric constant and loss at high frequency confirms the polarizing behavior of the candidate material.

V. REFERENCES

- [1]. Milliken R. S, J. Am. Chem. Soc. 72 (1950) 600.
- [2]. Smith G, Wermutha D, Healy P. C, Acta Cryst. E 60 (2004) 1800.
- [3]. Basoglu A, Avci D, Atalay Y, Elik F.C, Ahinbas T.S, Spectrochim. Acta Part A. 79 (2011) 1425.
- [4]. Haixia Ma, Biao Yan, Junfeng Li, Yinghui Ren, Yongshi Chen, Fengqi Zhao, Jirong Song, Rongzu Hu, J. Mol. Struct. 981(2010) 103.
- [5]. Janczak J, Perpétuo G. J, J. Mol. Struct. 975 (2010) 166.
- [6]. Sivaramkumar M. S, Velmurugan R, Sekar M, Ramesh P, Ponnuswamy M. N, Acta Cryst. E66 (2010) 1821.
- [7]. Jasinski J. P, Butcher R. J, Yathirajan H. S, Mallesha L, K. Mohana N, Acta Cryst. E65 (2009) 2365.
- [8]. Khan I. M, Ahmad A, Ullah M.F, J. Photochem. Photobio. B: Bio. 103(2011) 42.
- [9]. Singh N, Ahmad A, Can. J. Anal. Sci. Spec.54 (2009)1.
- [10]. Pande G.B, Shirodkar S.G, Joshi P.P, K.L. Kendre, Inter. Ind. & Ref. Res. 4 (2013) 40.
- [11]. Strzhemechny M. A, Baumer V.N, Avdeenko A. A, Pyshkin O. S, Romashkin R.V, Buravtseva L.M, Acta Cryst. B63 (2007)296.
- [12]. Safaei-Ghomi J, Fadaeian M, Hatami A, Turk J. Chem. 31(2007) 89.
- [13]. MHalla F, Pinson J, Saveant J.M, J.Electroanal. Chem. Interfac. Electrochem. 89 (1978) 347.
- [14]. Ravi M, Rao D.N, Cohen S, Agranat I, Radhakrishnan T.P, Chem.Mater.10 (1998) 2371-2377.
- [15]. GuruPrasad L, Krishnakumar V, Nagalakshmi R, PhysicaB405 (2010) 1652-1657.
- [16]. Frisch A, Nielson A.B, Holder A.J, GAUSSVIEW User Manual, Gaussian Inc, Pittsburgh, PA, (2000).
- [17]. Zhu M, Ma I, Zhang H, Analytical chemistry. 79 (2007) 8333-8341.
- [18]. Varsanyi. I. Acta Aliment. 1 (1972) 297-314.